Proceedings of Global Power and Propulsion Society
ISSN-Nr: 2504-4400
GPPS Hong Kong 2023
October 17-19, 2023
www.gpps.global

GPPS-TC-2023-0008

Performance Optimization For Pinwheel And Savonius Drag-Dominant Tidal Turbine Using Moment Balancing Method

Yixiao Zhang
Nanyang Technological University
yixiao002@e.ntu.edu.sg
Singapore, Singapore, Singapore

Shivansh Mittal
Nanyang Technological University
Shivansh001@e.ntu.edu.sg
Singapore, Singapore, Singapore

Eddie Ng Yin Kwee*
Nanyang Technological University
mykng@ntu.edu.sg
Singapore, Singapore, Singapore

ABSTRACT

Drag-dominated turbines play a key role in the application of urban windfarm and tidal arrays because of their low cut-in speed and omnidirectional characteristics. A performance analysis CFD study of Pinwheel and Savonius tidal turbines has been carried out. Disk Actuator model is found less suitable for DDTTs due to the varying swept area blockage, unaccounted bypass downstream flow interaction and rotor parasitic drag whereas Blade Element Momentum theory is computably effective for majorly 3-blade lift-dominated aero foil. This study proposes a novel method to find the optimal *TSR* of turbine with a cost-effective and user-friendly Moment Balancing algorithm. Dynamic *TSR* matrix was developed with varying rotational speeds and fluid velocities, unlike previous works simulated at a fixed fluid velocity. Novel parameters such as thrust and idle moment are introduced as functions of inlet fluid velocity and rotational speed respectively. These relationships are verified through regression analysis, and the turbines' net moment equations are established based on these parameters. Rotational speed was a reliable predictor for Pinwheel's idle moment, while inlet velocity was a reliable predictor for thrust moment in both models. The optimal (C_p, *TSR*) values for Pinwheel and Savonius turbines were (2.37, 0.223) and (0.63, 0.290) respectively, and lie within an acceptable for experimental validation.

INTRODUCTION

The potential of tidal energy as a reliable source of energy has been identified as a means of providing economic relief to communities located near coastlines or tidal channels. This energy source has the capacity to generate more than 130,000 terawatt-hours of electricity per year (IRENA, 2020). By utilizing smart grid infrastructure, the energy generated from tidal and wave technologies can be used to power residential, commercial, and tourism sectors, with the potential to meet 10% of the EU's power demand by 2050 (European Commission, 2020). For this purpose, drag-dominated tidal turbines (DDTTs) with simpler geometries and lower flow velocities are ideal for deployment in slow water currents. These turbines include axial or cross-flow turbines with a horizontal or vertical axis of rotation, respectively. The Disk Actuator model, which assumes the presence of a rotating virtual disc with or without porous holes perpendicular to the inflow direction around the rotor (Yilmaz & Meyers, 2014), is not suitable for use with vertical-axis turbines due to the varying sweep area of the rotor plate (Churchfield et al., 2017) and the unsteady effect of the unaccounted bypass flow interaction on the downstream wake for horizontal-axis turbines (Whelan, et al., 2009). Furthermore, it does not account for parasitic drag on the rotor and support walls in both turbine configurations (Muchala & Willden, 2017). Islam et al. (2019) applied the BEM theory through the Q-blade software and MATLAB script to optimize the design of a small horizontal axis wind turbine for low wind speed areas, however, the Blade Element Momentum (BEM) theory, which is computationally effective for lift-dominated aerofoils (Koh & Ng, 2016), is not suitable for drag-dominated tidal turbines (DDTTs) that are not always NACA-series type (Pucci, et al., 2022). Under these circumstances, other simulation techniques were utilised as supplementary tools.

Wihadi and Mardikus (2020) discovered that the 2-bladed single-stage Savonius tidal turbine exhibited the highest power coefficient in experimental comparisons with those possessing 3 or 4 blades. Patel et al. (2021) performed experimental investigations in a wind tunnel that verified an inverse correlation between performance and the overlap ratio, which denotes the proportion of the turbine blade overlap area to the total blade swept area. Kumar and Saini (2021) conducted experimental studies and numerical simulations to determine the optimal performance characteristics of a miniature Savonius turbine operating in a water channel with a low in-flow velocity of 0.5 m/s. The study revealed that the optimal *TSR* of 0.7 achieved the highest maximum power coefficient (C_P) value of 0.23. A 2 mm sheet thickness was implemented based on Salazar Marin and Rodríguez (2019). The performance enhancement of parabolic by Alipour et al. (2020) and Myring Equation-inspired blade designs by Tian et al. (2015) was investigated through two-dimensional transient simulations, while Gruber et al. (2012) analysed humpback whale-inspired

blade designs using ANSYS-CFX code. Islam et al. (2019) compared the performances of eleven different configurations of pinwheel wind turbines by Computational Fluid Dynamics (CFD) simulations and the Weibull distribution. Their study proposed a novel optimization strategy to improve blade design and power generation for DDTTs.

To summarize, Commercial solvers like Ansys Fluent utilizes the expensive and labor-intensive models to optimize turbine design by coupling them with complex mathematical programming for flow simulations. However, this approach increases the complexity of the solution, necessitating a more efficient method. Obtaining experimental validation for tidal turbines is a challenge for authors, as the required apparatus is significantly more expensive compared to wind tunnel equipment. This study introduced a new optimization method for improving the blade design and power generation of DDTTs. The proposed technique involved the integration of a cost-effective and user-friendly moment balancing algorithm, which combined the Moving Reference Frame (MRF) with hydrodynamic performance analysis. The authors examined the Pinwheel and Savonius turbine as two typical examples of DDTTs in this research. A preliminary result was presented to assist engineers in selecting from a broad range of computational techniques and to facilitate a better understanding of the optimization process.

In terms of error validation, this study investigated the following studies' result: (1) Nemoto and Ushiyama (2003) conducted experimental evaluations of pinwheel rotors with different cutting styles in a wind tunnel and found that as the number of blades increases, the Tip Speed Ratio (*TSR*) decreases, and the coefficient of power (C_P) is maximum for the 4-bladed rotor. Their findings suggested that an optimal *TSR* of 2.0, with a cut-in and cut-off speed of 1.65 m/s and 12.5 m/s, respectively, can be achieved; (2) Kumar and Saini (2021) conducted experimental studies and numerical simulations to determine the optimal performance characteristics of a miniature Savonius turbine operating in a water channel with a low in-flow velocity of 0.5 m/s. The study revealed that the optimal *TSR* of 0.7 achieved the highest maximum power coefficient (C_P) value of 0.23. (3) The numerical simulation results presented in the following sections demonstrate a good agreement with the experimental studies (Zhang, Mittal and E.Y.K. Ng, 2023).

METHODOLOGY

Model scaling and boundary conditions

The CFD simulation domains of the Pinwheel and Savonius models are created by conducting a parametric study to equalize the blockage ratio of both models. The blockage ratio is the area occupied by the blades to the turbine inlet area whereas the aspect ratio is the ratio of a turbine blade's length to the radius of the rotor. Identical simulation data from Kumar & Saini (2021) of the Savonius and channel scales are chosen to calculate the fixed aspect ratio at 1.85. This value is then set to be equivalent to the Pinwheel turbine's channel scale and area, as given in *Eq.*(3)-(5). Then a common blockage at 12% for both turbines is calculated as the ratio of blade area to channel area.

$$Aspect\ Ratio\ (\text{Savonius}) = \frac{Channel\ Width\ = 0.600}{Channel\ Height\ =\ 0.325} = 1.85 \tag{1}$$

$$Channel\ Area\ (Savonius) =\ Channel\ Width.Channel\ Height\ =\ (0.600\ m).(0.325\ m)\ = 0.195\ m^2 \tag{2}$$

Then, these are applied to the Pinwheel's domain for as given in *Eq* (3) and (4).

$$Aspect\ Ratio\ (\text{Pinwheel}) = \frac{Channel\ Width\ (X)}{Channel\ Height\ (Y)} = 1.85 \tag{3}$$

$$Channel\ Area\ (Pinwheel) =\ Channel\ Width\ (\text{X}).Channel\ Height\ (Y)\ = 2.36\ \text{m}^2 \tag{4}$$

Upon multiplying LHS and RHS of *Eq.*(3) by Y as given in *Eq.*(5) and substituting Y in *Eq.* (4), the Pinwheel channel width and height can be calculated as $(\text{X}, \text{Y}) = (2.09, 1.13)$ m.

$$\frac{\text{X}}{Y}.\frac{Y}{Y} = \frac{2.36}{Y^2} = 1.85, thus, Y = \sqrt{\frac{2.36}{1.85}}\ =\ 1.13\ m \tag{5}$$

Under the same aspect ratio and blockage, the significant lengths are calculated as the ratio of 4 times the channel cross-section area to wetted perimeter of the rectangular channel, equal to 1.4658 m for Pinwheel and 0.4216 m for Savonius. By identifying the velocity ranges from 0.4 m/s to 1.0 m/s for Pinwheel and from 0.33 m/s to 0.83 m/s for Savonius; and the dynamic viscosity is 0.00103 Pa·s in Table 1, the flow field's Reynolds number (*Re*) can be obtained from the different flow speed ranges.

Table 1: Scales of the CFD Models and properties of fluid in CFD models

Parameter	Unit	Pinwheel	Savonius	Parameter	Unit	Pinwheel	Savonius
Blade Radius	m	0.3	0.059	Channel Height	m	1.13	0.325
Rotor Diameter	m	0.6 (*D*)	0.118 (*a*)	Channel Area	m^2	2.36	0.195
Rotor Height	m	0.6	0.187 (*b*)	Aspect Ratio	/	**1.85**	**1.85**
End-Plate Diameter	m	-	0.130	Blockage Ratio	/	**0.12**	**0.12**
Blade Area	m^2	0.283	0.022	Min *Re*	/	542k	129k
Channel Width	m	2.09	0.600	Max *Re*	/	1354k	323k

Figure 1 gives the overview of volume mesh for both turbines and specifically the Pinwheel turbine was simulated with a grid consisting of 2,080,945 cells, which was determined based on a fluid velocity of 0.9 m/s, rotational velocity of 7.5 rad/s, and *TSR* of 2.5. Meanwhile, the Savonius turbine utilized a grid with 1,069,955 cells, selected according to a fluid velocity of 0.5 m/s, rotational velocity of 6 rad/s, and *TSR* of 0.7. The *K-ε* turbulence steady-state segregated solver with a continuity criterion set to residuals of magnitude 10^{-3} was utilized for both simulations, which enables easy comparisons of the C_p-*TSR* performance curve simulation findings. Grid independence is tested as Figure 2 for both turbines where 2.0 and 1.0 million grid numbers are selected for Pinwheel and Savonius respectively.

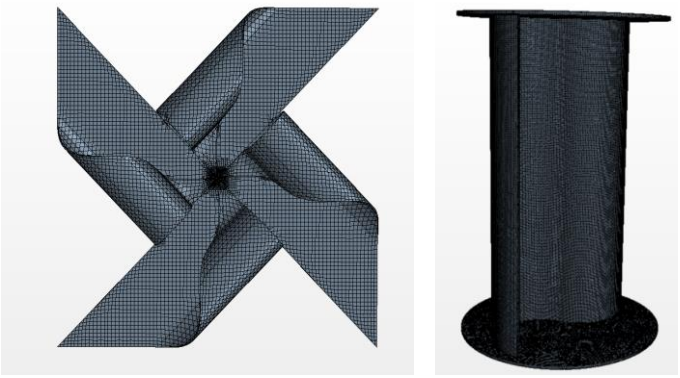

Figure 1: Volume mesh overview for (a) Pinwheel and (b) Savonius turbine

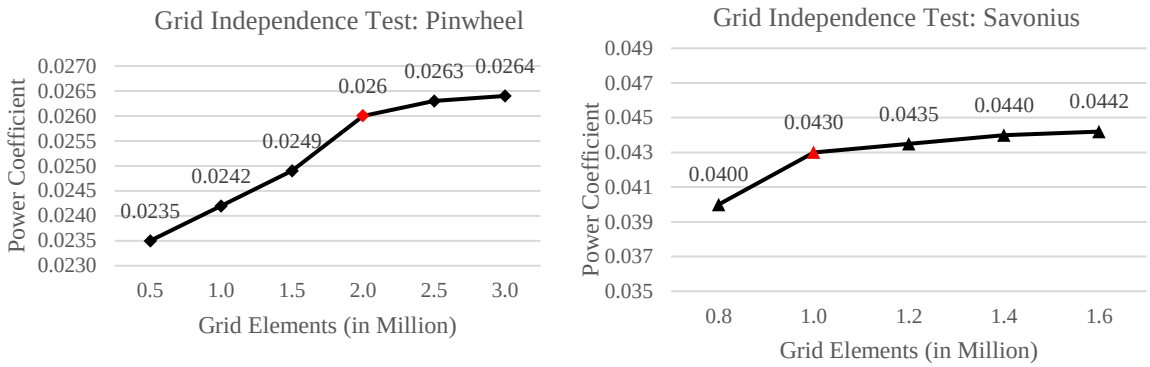

Figure 2: Grid Independence Study for (a) Pinwheel and (b) Savonius turbine

Turbulence equations:

In this study, the Segregated Solver is employed to discretize and solve the mass and momentum integral conservation equations. The near wall function for calculating dimensionless *y+* selected blending approach wherein it emulates low wall treatment for fine grids and high wall treatment for coarse grids.

For the simulations conducted in STAR-CCM+, the Realizable K-Epsilon with Two-Layer (RKE 2L) method was selected as the turbulence model. The RKE 2L determines the turbulence dissipation rate (ε) and turbulence viscosity (μ_t) as a function of the distance from the wall in the near-wall layer followed by $\mu_t = \rho C_\mu f_\mu (k^2/\varepsilon)$ where the model coefficient C_μ is set at 0.9 and damping coefficient f_μ is 1.0 in RKE 2L. These values are seamlessly integrated with the results obtained from solving the transport equations in regions away from the wall. Then the *k* and *ε* are obtained from the following transport equations *Eq.*(6) and *Eq.*(7) where the velocity and direction are derived along the x direction:

$$\frac{\partial(\rho k)}{\partial t} + \frac{\partial(\rho k U_i)}{\partial x_i} = \frac{\partial}{\partial x_i}\left[\left(\mu + \frac{\mu_t}{\sigma_k}\right)\frac{\partial k}{\partial x_i}\right] + f_c G_k + G_b - \rho\varepsilon - Y_M + S_k \tag{6}$$

$$\frac{\partial(\rho \varepsilon)}{\partial t} + \frac{\partial(\rho \varepsilon U_i)}{\partial x_i} = \frac{\partial}{\partial x_i}\left[\left(\mu + \frac{\mu_t}{\sigma_\varepsilon}\right)\frac{\partial \varepsilon}{\partial x_i}\right] + C_{1\varepsilon}\varepsilon - C_{2\varepsilon}\frac{\rho\varepsilon^2}{k + \sqrt{U_i \varepsilon}} + \frac{\varepsilon}{k} C_{3\varepsilon} G_b + S_\varepsilon \tag{7}$$

Where, G_k -Turbulent kinetic energy generation coefficient; G_b -Turbulence dissipation rate generation coefficient; Y_M-Specific dissipation rate to turbulent kinetic energy ratio; S_k, S_ε-User-defined source terms; $C_{1\varepsilon}$, $C_{2\varepsilon}$, $C_{3\varepsilon}$- Constants, equal to $\max(0.43, Sk/5\varepsilon + Sk)$;$\sigma_k$, σ_ε-Turbulent Prandtl numbers, equal to 1.0 and 1.2 respectively in RKE 2L.

Derivation of Characteristic Equation

Moment analysis of a single turbine configuration has been investigated in either horizontal or vertical axis cases. This study introduces two new moment definitions, the Idle and Thrust moments, derived mathematically from previous literature equations with respect to ICs, i.e., the rotational velocity ω and fluid velocity U_1. The aim is to establish an equilibrium state and describe its moment balancing equation to determine the optimal power coefficient $C_{p,opt}$. Prior research utilized a fixed inlet flow speed scheme however, this study employs a dynamic *TSR* matrix for the simulations.

Net Moment Balancing Equation:

Hara and Hayashi, (2012) studied the performance dependence of VAWTs on the moment of inertia in an unsteady wind tunnel, and proposed *Eq.*(8) with the net angular momentum ΔL as a sum of torque of wind turbine τ_w, brake τ_B and load τ_L. Ordonez-Sanchez et al. (2019) proposed *Eq.*(9) for calculating the net torque on a turbine under a set optimal rotational speed operation as the motor generates a counterbalancing torque on turbine rotor under fluid loading.

$$\Delta L = I\frac{dw}{dt} = (\tau_w - \tau_B) - \tau_L \tag{8}$$

$$J\ddot{\theta} = \tau_{Rotor} - D(\dot{\theta}) - \tau_{Motor} \tag{9}$$

The net moment when the turbine is stationary, but the fluid motion exerts load to rotate the turbine, is defined as the thrust moment, $M_{Thrust}(U_1, 0)$, governed by thrust coefficient C_T and fluid velocity U_1. Idle moment, $M_{Idle}(0, \omega)$, is defined when the turbine is rotating at constant speed in still water hence, a load is exerted on the turbine. It is governed by the viscosity and centrifugal force of the fluid. Applying the principle of conservation of angular momentum and assuming steady operation in *Eq.*(8), the sum of the external moments $(\Sigma\tau)$ is zero as derived in *Eq.*(10) or the form of Moment Balancing equation in *Eq.*(11):

$$\Sigma\tau = \Delta L = \tau_w - (\tau_L + \tau_B) = 0 \tag{10}$$

$$M_{net,opt}(U_1, \omega) = M_{Thrust}(U_1, 0) + M_{Idle}(0, \omega) = 0 \tag{11}$$

Where the thrust moment is the torque generated by the wind turbine i.e., $M_{Thrust} = \tau_w$ and the idle moment is equal to the sum of the load torque and the braking torque i.e., $M_{Idle} = \tau_L + \tau_B$. In the case of the horizontal axis Pinwheel turbine, the simulation result finds that the braking torque τ_B is zero, thus noted as ${M_{Idle}}^*$.

Also from *Eq.*(9), assuming steady operation and negating damping factor D, it is found that the torque produced by the motor i.e., $\tau_{Motor} = M_{Idle}$ counterbalances the torque experienced by the rotor blades i.e., $\tau_{Rotor} = M_{Thrust}$ during steady operation in the tank. This indicates that the optimal power performance is achieved when $M_{net,opt}$ is zero, i.e., the neutral point, where the thrust and idle moment equally offset. The significance of Moment Balancing equation is to replace the unsteady cyclic volume force analysis with a simplified steady moment analysis. This method is useful in simulations for determining the values of U_1 and ω to achieve equilibrium. Engineers can determine the optimal power coefficient by observing their model results for the net moment approaching zero, indicating a neutral point where Idle and Thrust moment are equal and can be used interchangeably to calculate the power coefficient using *Eq.*(12).

$$C_{p,opt} = \frac{P_{extracted}}{P_{in}} = \frac{\omega \cdot M_{Thrust/Idle}}{\frac{1}{2}\rho A {U_1}^3} \tag{12}$$

Thrust and Idle Moment Equation:

The following mathematical derivations demonstrates the reason why thrust and idle moment are solely dependent on U_1 or ω respectively. The equations for deriving the moment on a rotor plate due to the thrust force are given in *Eq.* (13).

$$M_{Thrust} = F_{Thrust}.l = \frac{1}{2}\rho A C_T {U_1}^2 \times l = \begin{cases} (\frac{\rho\pi D^3 C_T}{16}) \cdot {U_1}^2 & (Pinwheel) \\ (\frac{\rho a b C_T}{2}) \cdot {U_1}^2 & (Savonius) \end{cases} \tag{13}$$

Hereby the M_{Thrust} is linearly related to only the ${U_1}^2$. In a steady state and incompressible flow, for the Idle moment, it is governed by the modified Navier-Stokes Momentum equations in rotational frame (Menon et al.) in *Eq.*(14) with the additional centrifugal force terms. In steady state with static inflow velocity, the M_{Idle} is expressed as the force arm $\boldsymbol{r}$ times the sum of pressure difference and the centrifugal force's term indicated as *Eq.*(15). Hereby the M_{Idle} is linearly related to only the ω^2.

$$\rho(\frac{\partial \boldsymbol{U_1}}{\partial t} + \boldsymbol{U_1}\nabla^2\boldsymbol{U_1}) = -\nabla\boldsymbol{P} + \mu\nabla^2\boldsymbol{U_1} + \rho(\omega^2 r + 2\omega\boldsymbol{U_{rotational}}) \tag{14}$$

$$M_{Idle} = \int(\int \boldsymbol{P}dA + \int \boldsymbol{\tau}dA)d\boldsymbol{r} \tag{15}$$

Dynamic TSR Matrix:

The two varying independent variables i.e., U_1 and ω comprise a dynamic *TSR* matrix using *Eq.*(16), shown for both turbines as Table 2(a) and (b). The turbine's optimal *TSR* can be obtained by the C_p-*TSR* curve.

$$TSR = \frac{\omega R}{U_1} \tag{16}$$

Table 2(a): Dynamic *TSR* matrix in different ICs for Savonius rotor

TSR		Rotational speed $\boldsymbol{\omega}$ (rad/s)								
		4.50	5.00	5.25	5.50	5.75	6.00	6.25	6.50	6.75
Inlet speed	0.33	0.80	0.89	0.94	0.98	1.03	1.07	1.12	1.16	**1.21**
	0.42	0.63	0.7	0.74	0.77	0.81	0.84	0.88	**0.91**	0.95
	0.46	0.58	0.64	0.67	0.71	0.74	0.77	**0.8**	0.83	0.87

U_1 (m/s)										
	0.50	0.53	0.59	0.62	0.65	0.68	**0.71**	0.74	0.77	0.80
	0.54	0.49	0.55	0.57	0.60	**0.63**	0.66	0.68	0.71	0.74
	0.58	0.46	0.51	0.53	**0.56**	0.58	0.61	0.64	0.66	0.69
	0.67	0.40	0.44	**0.46**	0.48	0.51	0.53	0.55	0.57	0.59
	0.75	0.35	**0.39**	0.41	0.43	0.45	0.47	0.49	0.51	0.53
	0.83	**0.32**	0.36	0.37	0.39	0.41	0.43	0.44	0.46	0.48

Table 2(b): Dynamic *TSR* matrix in different ICs for Pinwheel rotor

TSR		Rotational speed ω (rad/s)			
		6.67	7.50	8.00	8.17
Inlet speed U_1 (m/s)	0.40	**0.80**	0.80	0.79	0.81
	0.50	1.08	**1.15**	1.16	1.19
	0.60	1.49	1.52	**1.55**	1.57
	0.70	1.94	1.99	2.03	**2.06**
	0.80	2.56	2.57	**2.58**	2.62
	0.90	3.26	**3.23**	3.26	3.29
	1.00	**4.18**	4.02	4.00	4.03

RESULTS AND DISCUSSION

Idle and Thrust moment relationship quadratic with U_1 and ω

For internal validation of the simulation findings, the regression equations for the Idle and Thrust moment were calculated using Multi-Variate Linear Regression analysis in Microsoft Excel and the goodness of fit of the regression model was tested by the R^2 value. Rotational speed of the Pinwheel was found to be an exceptional predictor variable, with $R^2 \approx 1$. However, in the case of Savonius, it was a weak predictor owing to a low $R^2 \approx 0.25$ as given in Figure 3.

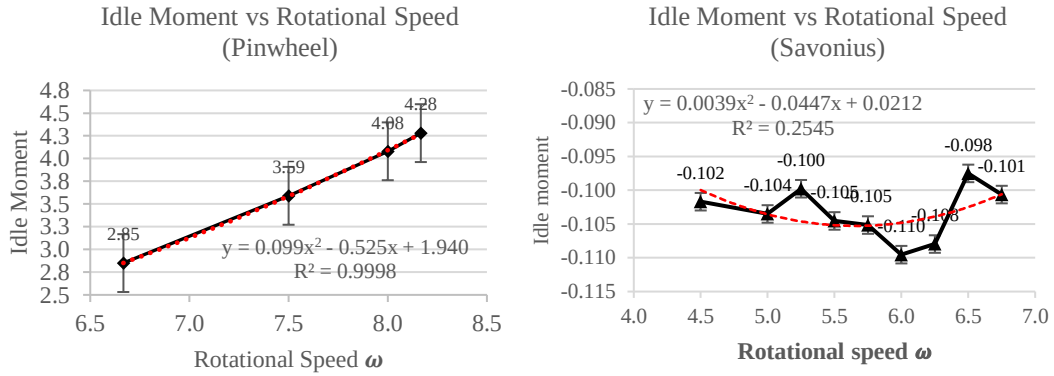

Figure 3: $M_{idle} - \omega$ quadratic relationship for (a) Pinwheel and (b) Savonius turbine

For thrust moment, inlet velocity was found to be an exceptional predictor variable for both models, with an $R^2 \approx 1$ as given in Figure 4. Hence, to calculate the optimal power coefficient, thrust moment's regression equation is selected.

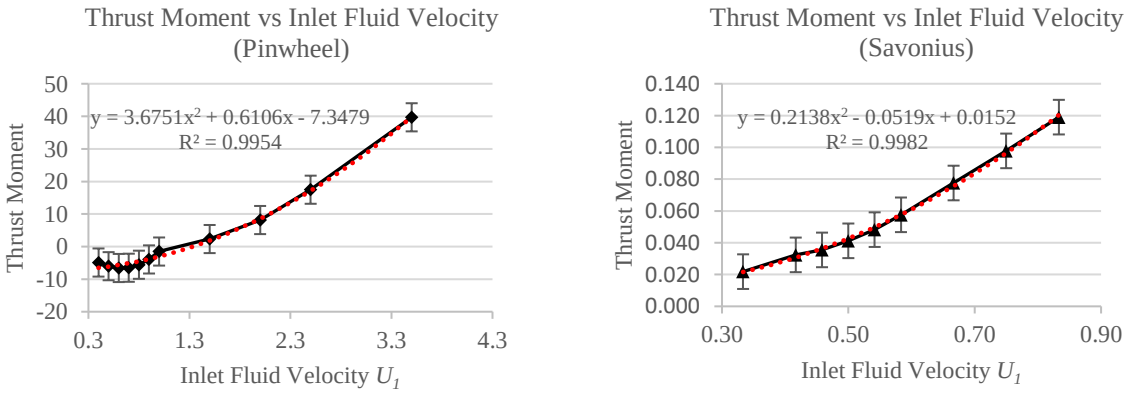

Figure 4: $M_{Thrust} - U_1$ quadratic relationship for (a) Pinwheel and (b) Savonius turbine

The two moments were selected as independent variables and the net moment as dependent variable. The algebraic equation of thrust and idle moment with net moment is defined as the Net Moment Balancing Equation for calculating corresponding turbine's power coefficient in Table 3.

Note that for Pinwheel, the $\boldsymbol{M_{Idle}}^*$ is the moment recorded by the simulation, while for Savonius, $\boldsymbol{M_{Idle}}$ is intercepted with the braking torque of -0.0812 N.m. This offset value represents the counterbalancing negative and positive torque during the intrinsic rotation of the VATs. ϵ is the relative uncertainty term produced by the second order polynomial regression and is smaller than 5% for both. The fluid flow characteristics can be compared in the two models based on the same blockage and aspect ratio. The difference in the two models lies in the $\boldsymbol{M_{Idle}}^*$ intercept for the VATs and the gradient of the net moment equation. These differences cause lower C_p for the Savonius than the Pinwheel turbine.

Table 3: Characteristic Net Moment Balancing Equation for Pinwheel and Savonius turbine

Equations	Model
$\boldsymbol{M_{Net}} = (1.0)\,\boldsymbol{M_{Thrust}} + (1.0)\,\boldsymbol{M_{Idle}}^* + \epsilon$	Pinwheel
$\boldsymbol{M_{Net}} = (0.85)\,\boldsymbol{M_{Thrust}} + (0.85)\,\boldsymbol{M_{Idle}} + \epsilon$	Savonius

Moment plots

The relationship between the three moments is visualized in the Figure 5 (a) and (b). It can be demonstrated that the Idle moment exhibits minimal deviation from a constant value with the growth of *TSR*, whereas the thrust moment curve closely adheres to the shape of the net moment curve. The rotor's balanced state is represented when net moment is zero, that is, the neutral point of the simulation.

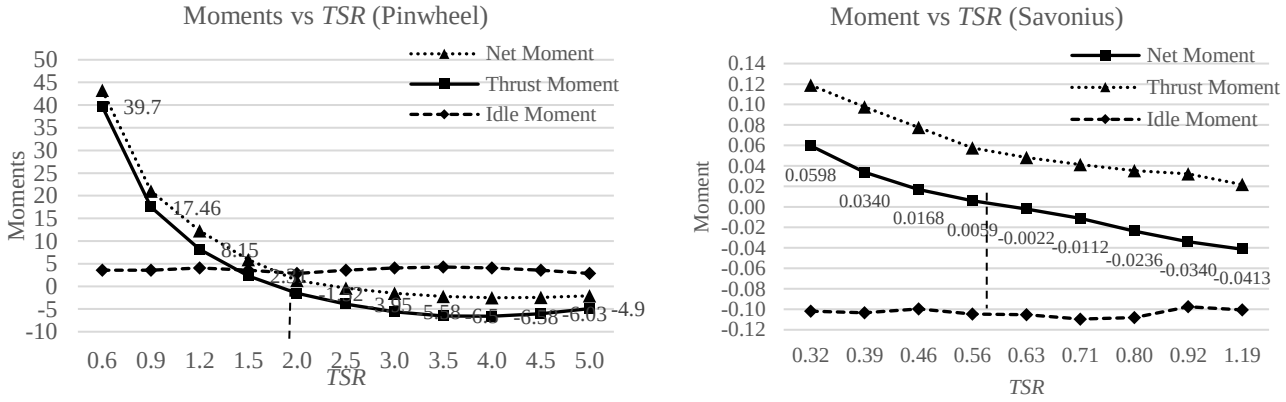

Figure 5: Net, Thrust and Idle Moment curves with the neutral point for (a) Pinwheel and (b) Savonius

Error by external validation

For the external validation of the simulation findings, the optimal C_p and *TSR* are found and compared with the reference studies for Pinwheel and Savonius which lie in the acceptable range of experimental validation. The results are summarised in Table 5.

Table 5: Characteristic Net Moment Balancing Equation for Pinwheel and Savonius turbine

Model	Reference Study	Simulation Result	Error Percentage
Pinwheel	2.0 (Nemoto, Y. et al. 2003)	2.37 (Optimal *TSR*)	$(\frac{2.37-2.0}{2.37})\times100 = 15.6\%$
	0.17 (Nemoto, Y. et al. 2003)	0.223 (Optimal C_p)	$\left(\frac{0.223-0.17}{0.223}\right)\times100 = 23.8\%$
Savonius	0.7 (Kumar and Saini, 2021)	0.63 (Optimal *TSR*)	$(\frac{0.63-0.7}{0.63})\times100 = 10.0\%$
	0.23 (Kumar and Saini, 2021)	0.29 (Optimal C_p)	$(\frac{0.29-0.23}{0.29})\times100 = 20.7\%$

Blade Load Distribution by Pressure Analysis

The difference of pressure plots shows the thrust and idle moment. In the front view in Figure 6, the thrust moment on the blade tip's leading-edge pressure is opposite to that of the root of trailing edge. The flapwise bending moment will be forward (blue arrow) and backward (red arrow) at the corresponding places. While in Figure 7(a), half of the Savonius' blade is fully negative pressure while the other half is positive. The cyclic moment is more suitable for unsteady solver making the Savonius idle moment result less correlated with the square of rotational speed ω^2.

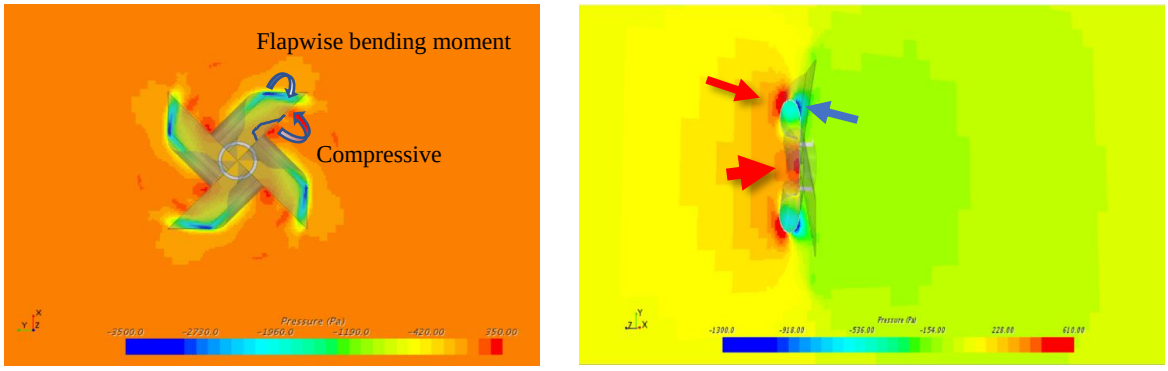

Figure 6: Pressure scalar plots of the front view (a), and lateral view (b) of Pinwheel, TSR_{opt}=2.731

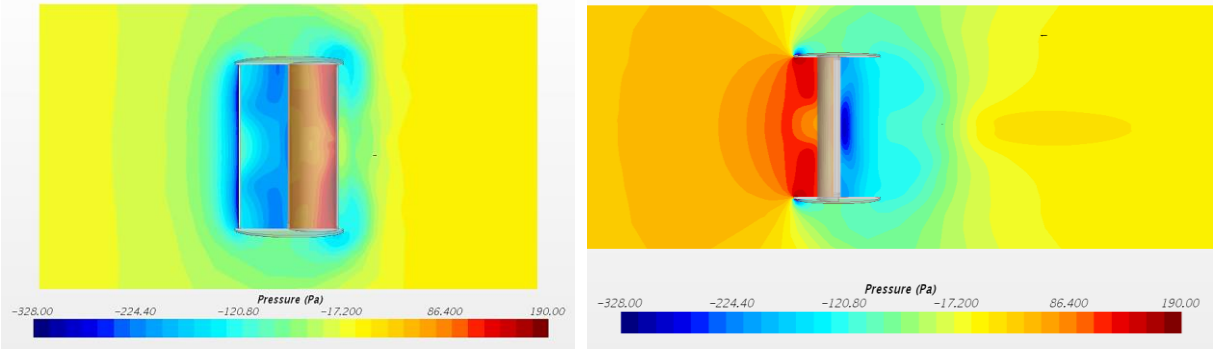

Figure 7: Pressure scalar plots of the front view (a), and lateral view (b) of Savonius, TSR_{opt}=0.63

CONCLUSION

This study has successfully established the algebraic equations between newly introduced parameters with the net moment on a turbine. It is found that at the neutral point, idle and thrust moment will offset each other in the optimal state. By this method, the optimal *TSR* and C_p for Pinwheel turbine is 2.37 and 0.223, and for Savonius turbine is 0.63 and 0.29, with the validation against two experiments at an understandable error rate at (15.6%, 23.8%) and (10%, 20.7%) respectively. Rotational speed was found to be an excellent predictor for Pinwheel's idle moment, while the inlet velocity was an excellent predictor for thrust moment in both models. Significance of the method, newly designed turbine blade, feasible way to supplement Disk actuator theory and BEM with less computational cost.

NOMENCLATURE

List of key terms, acronyms, and symbols:

λ	Tip Speed Ratio	$M_{thrust/idle}$	Moment of thrust and idle
ρ	Density of Liquid, kg/m^3	*Re*	Reynolds number
ω	Turbine's rotation speed, rad/s	*K-ε*	Kappa-Epsilon Turbulence Model
μ	Dynamic Viscosity, Pa.s	*K-ω*	Kappa-Omega Turbulence Model
R	Rotor radius, m	SST	Shear-Stress Transport Turbulence Model
U_1	Inflow speed, m/s	VATs	Vertical Axis Turbines
A	Cross-section area of a rotor plate, m^2	DDTTs	Drag-Dominant Tidal Turbines
C_P	Power Coefficient	BEM	Blade Element Method
C_T	Thrust Coefficient	MRF	Moving Reference Frame
I	Moment of Inertia, kg.m^2	EU	European Union
L	Angular momentum, kg.m^2/s	DDTTs	Drag-dominated tidal turbines
$\tau_w\ \tau_B\ \tau_L$	Turbine torque of wind, brake and load	CFD	Computational Fluid Dynamics

ACKNOWLEDGMENTS

The authors would like to thank Nanyang Technological University for providing the computing facilities as needed to carry out this study, as well as the Interdisciplinary Graduate School scholarship for funding this project. The authors would also like to thank Prof. Jiang Wei of Wuhan University (WHU) and Prof. Zou Zhengping of Beihang University (BUAA) for their valuable contribution in discussions regarding the inspirations of the methodologies.

REFERENCES

Alipour, R., Alipour, R., Fardian, F., Koloor, S.S.R. and Petrů, M. (2020). Performance improvement of a new pro posed Savonius hydrokinetic turbine: a numerical investigation. Energy Reports, 6, pp.3051–3066. doi:https://doi.org/10.10 16/j.egyr.2020.10.072.

Biswas, A., Gupta, R. and Sharma, K.K. (2007). Experimental Investigation of Overlap and Blockage Effects on Th ree-Bucket Savonius Rotors. Wind Engineering, 31(5), pp.363–368. doi:https://doi.org/10.1260/030952407783418702.

Churchfield, M.J., Schreck, S.J., Martinez, L.A., Meneveau, C. and Spalart, P.R. (2017). An Advanced Actuator Lin e Method for Wind Energy Applications and Beyond. 35th Wind Energy Symposium. doi:https://doi.org/10.2514/6.2017-1 998.

European Commission (2020). Tidal flows generate huge potential for clean electricity | Research and Innovation. [o nline] ec.europa.eu. Available at: https://ec.europa.eu/research-and-innovation/en/projects/success-stories/all/tidal-flows-genera te-huge-potential-clean-electricity.

Gruber, T., Murray, M.M. and Fredriksson, D.W. (2012). Effect of Humpback Whale Inspired Tubercles on Marine Tidal Turbine Blades. [online] asmedigitalcollection.asme.org. doi:https://doi.org/10.1115/IMECE2011-65436.

Hara, Y., Hara, K. and Hayashi, T. (2012). Moment of Inertia Dependence of Vertical Axis Wind Turbines in Puls ating Winds. International Journal of Rotating Machinery, 2012, pp.1–12. doi:https://doi.org/10.1155/2012/910940.

IRENA (2020). Innovation outlook: Ocean energy technologies. https://www.irena.org/. Abu Dhabi: International Ren ewable Energy Agency.

Islam, Md.R., Bin Bashar, L., and Rafi, N.S. (2019). Design and Simulation of A Small Wind Turbine Blade with Qblade and Validation with MATLAB. 2019 4th International Conference on Electrical Information and Communication Technology (EICT). doi:https://doi.org/10.1109/eict48899.2019.9068762.

Islam, R., Sultana Snikdha, Z., Iffat, A. and Shahadat, M.Md.Z. (2021). Optimum Blade Design of Pinwheel Type Horizontal Axis Wind Turbine for Low Wind Speed Areas. [online] IEEE Xplore. doi:https://doi.org/10.1109/ACMI5387 8.2021.9528222.

Koh, W.X.M. and Ng, E.Y.K. (2016). Effects of Reynolds number and different tip loss models on the accuracy of BEM applied to tidal turbines as compared to experiments. Ocean Engineering, [online] 111, pp.104–115. doi:https://do i.org/10.1016/j.oceaneng.2015.10.042.

Kumar, A. and Saini, G. (2021). Flow field and performance study of Savonius water turbine. Materials Today: Pro ceedings, 46, pp.5219–5222. doi:https://doi.org/10.1016/j.matpr.2020.08.591.

Menon, Sananth H., et al. "Derivation of Navier–Stokes Equation in Rotational Frame for Engineering Flow Analysi s." *International Journal of Thermofluids*, vol. 11, Aug. 2021, p. 100096. *ISSN 2666-2027*, https://doi.org/10.1016/j.ijft.20 21.100096. Accessed 1 May 2022.

Muchala, S. and Willden, R.H.J. (2017). Impact of tidal turbine support structures on realizable turbine farm power. Renewable Energy, 114, pp.588–599. doi:https://doi.org/10.1016/j.renene.2017.07.002.

Nemoto, Y. and Ushiyama, I. (2003). Experimental Study of a Pinwheel-Type Wind Turbine. Wind Engineering, 27 (3), pp.227–236. doi:https://doi.org/10.1260/030952403769016708.

Ordonez-Sanchez, S., Allmark, M., Porter, K., Ellis, R., Lloyd, C., Santic, I., O'Doherty, T. and Johnstone, C. (201 9). Analysis of a Horizontal-Axis Tidal Turbine Performance in the Presence of Regular and Irregular Waves Using Tw o Control Strategies. Energies, 12(3), p.367. doi:https://doi.org/10.3390/en12030367.

Patel, V. and Patel, R. (2021). Energy extraction using modified Savonius rotor from Free-flowing water. Materials Today: Proceedings, 45, pp.5190–5196. doi:https://doi.org/10.1016/j.matpr.2021.01.703.

Pucci, M., Di Garbo, C., Bellafiore, D., Zanforlin, S. and Umgiesser, G. (2022). A BEM-Based Model of a Horizo ntal Axis Tidal Turbine in the 3D Shallow Water Code SHYFEM. Journal of Marine Science and Engineering, 10(12), p.1864. doi:https://doi.org/10.3390/jmse10121864.

Salazar Marin, E.A. and Rodríguez, A.F. (2019). Design, assembly and experimental tests of a Savonius type wind turbine. Scientia et Technica, 24(3), pp.397–407. doi:https://doi.org/10.22517/23447214.20411.

Tian, W., Song, B., VanZwieten, J. and Pyakurel, P. (2015). Computational Fluid Dynamics Prediction of a Modifie d Savonius Wind Turbine with Novel Blade Shapes. Energies, 8(8), pp.7915–7929. doi:https://doi.org/10.3390/en8087915.

Whelan, J.I., Graham, J.M.R. and Peiro, J. (2009). A free-surface and blockage correction for tidal turbines. Journal of Fluid Mechanics, [online] 624, pp.281–291. doi:https://doi.org/10.1017/s0022112009005916.

Wihadi, D. and Mardikus, S. (2020). Experimental investigation of blades number of savonius water turbine on perf ormance characteristic. The 5th International Conference on Industrial, Mechanical, Electrical, and Chemical Engineering 2019 (ICIMECE 2019). doi:https://doi.org/10.1063/5.0001063.

Yang, B. and Lawn, C. (2011). Fluid dynamic performance of a vertical axis turbine for tidal currents. Renewable Energy, 36(12), pp.3355–3366. doi:https://doi.org/10.1016/j.renene.2011.05.014.

Yilmaz, A.E. and Meyers, J. (2014). Numerical simulations of flow fields through conventionally controlled wind tu rbines & wind farms. Journal of Physics: Conference Series, 524, p.012158. doi:https://doi.org/10.1088/1742-6596/524/1/0 12158

Zhang, Y., Mittal, S. and Ng, E.Y.-K. (2023). CFD Validation of Moment Balancing Method on Drag-Dominant Ti dal Turbines (DDTTs). Processes, 11(7), p. 1895. Available at: https://doi.org/10.3390/pr11071895.

Zhang, Y., Mittal, S. and Ng, E.Y.K. (2023). Simulation validation of moment balancing method for drag-dominant tidal turbines, in dr.ntu.edu.sg. 15th International Green Energy Conference (IGEC-XV). Available at: https://hdl.handle.n et/10356/169199 (Accessed: 23 August 2023).